Spatio-Temporal Correlations in Thermal Avalanches

Sylvain Mortgat, Supervisor: Tom de Geus

July 3, 2024

1 Introduction

The concept of depinning finds application in a variety of fields, ranging from the study of crack propagation in disordered media to the movement of magnetic domain walls in ferromagnetic materials, and the dynamics of earthquakes. It describes how interfaces move through disordered environments. Depinning occurs when an external force f exceeds a certain threshold f_c, triggering motion. At $f = f_c$, this motion is characterised by sudden and collective reorganisations known as avalanches. For $f < f_c$, the movement of the interface is mainly driven by thermal fluctuations that provide enough energy to jump over the pinning potential barriers. In this report, we are interested in sequences of reorganisations induced by thermal fluctuations, called *thermal avalanches*. More precisely, we try to explore a parallel between our model and the physics of earthquakes. In section 2, we begin with a description of the model, which originates from [1]. We define *thermal avalanches* as a sequence of yielding events that follow each other in short succession: within a duration $\Delta t < \tau_0$, where τ_0 is a characteristic time chosen as a fraction of the interface's relaxation time τ_α. Then, we define *mainshocks* and *aftershocks*. In section 3, we graphically explore the results of our definitions. Finally, we examine the Omori-Utsu law, which describes the decay frequency of aftershocks, and check whether it holds true within the context of our model.

2 Model

2.1 General description

The system is modelled as a cubic cellular automaton with periodic boundary conditions, consisting of L^d blocks (or cells). Here, L represents the linear size, and d represents the dimension of the system. Each cell, denoted as i, is subject to an external driving force f_i and has a yielding threshold f_i^y. This configuration allows us to define the distance to yielding for each cell as $x_i := |f_i| - f_i^y$. At a finite temperature $T > 0$, the dynamics use this quantity to determine which block fails, it is analogous to the role of activation energy. Specifically, the failing block i is the one with the smallest time to failure τ_i, which is given by $\tau_i = \tilde{\tau} \exp(-x_i^\alpha / T)$ for unstable blocks ($x_i \geq 0$), and $\tau_i = \tilde{\tau}$ for stable ones ($x_i < 0$). Here, the Boltzmann constant is absorbed in the temperature. When a block fails, it first loses its force such that $f_i(t + \Delta t) = f_i(t) - \Delta f_i = \epsilon$, where ϵ is a small number drawn from a normal distribution. Subsequently, the force drop $\Delta f_i = f_i(t) - \epsilon$ is uniformly redistributed to the 2^d nearest neighbours of i. If $j(i)$ denotes the j-th nearest neighbour of i, then $f_{j(i)}(t + \Delta t) = f_{j(i)}(t) + \Delta f_i / 2^d$. This means that the system is driven by a constant force $f = \sum_i f_i / L^d$ which is kept equal to $f_c/2$ at all times. Here, f_c denotes the critical force at which the interface undergoes a depinning transition. Finally, the position of the failing block is updated as $u_i(t + \Delta t) = u_i(t) + \Delta f_i / k$, with the elastic constant k set to 1. Measurements are collected once a steady state is reached.

2.2 Implementation details

The model is implemented in the `GooseEPM` package [2]. A $d = 2$ dimensional system from the `SystemThermalStressControl` class is instantiated with $L = 512$, $\alpha = 3/2$, $\tilde{\tau} = 1$ and the `laplace_propagator` is used for nearest neighbour interactions. The temperature is set at $T = 0.002$. Each block i has a yielding threshold f_i^y, which is non-negative and determined by sampling from a truncated normal distribution with a mean $\bar{f}^y = 1$ and a standard deviation $\sigma_{f^y} = 0.3$. Upon failure, a block's force is reduced to a value ϵ which is drawn from a normal distribution with a mean 0 and a standard deviation 0.01. The position and time of failure of each failing block is tracked throughout the simulation. The constant driving force f is set to $0.3 \approx f_c/2$. The critical force f_c is established by driving the system athermally and quasi-statically using a weak spring. During system initialisation, each block is assigned a force f_i sampled from a normal distribution with a mean f and a standard deviation $\sigma_{f_i} = 0.1$. The system is iteratively updated by failing unstable blocks until all blocks are stable. To reach a steady state, the dynamics are run for $100L^d$ steps. Subsequently, data is collected in segments of $N_{\text{steps}} := 20L^d$ steps for analysis.

2.3 Defining avalanches, mainshocks and aftershocks

Relaxation time τ_α. The macroscopic relaxation time of the system, τ_α, is defined as the time needed to fail half of the system, i.e. $L^d/2$ different blocks. To determine τ_α, we run the system's dynamics over N_{steps} steps. Each time the count of distinct blocks that have failed exceeds $L^d/2$, we record the corresponding time $t_\alpha^{(i)}$, reset the count and measure the time until the next occurrence of $L^d/2$ block failures. The macroscopic relaxation time τ_α is computed as the average of these consecutive time intervals, i.e. $\tau_\alpha = \langle t_\alpha^{(i)} \rangle \approx 6.17 \times 10^{135}$.

Avalanche segmentation and time threshold τ_0. To segment the sequence of events into avalanches, we define a temporal threshold τ_0. We consider two consecutive block failures as part of the same avalanche if the time difference Δt between them is less than τ_0. Once we establish τ_α, we set τ_0 as a fraction of this value, fine-tuned to effectively distinguish between individual avalanches. In addition to recording the position and time of block failures, avalanches are characterised by two quantities: the extent A, which corresponds to the number of unique blocks that yield in each avalanche, and the size of the avalanches, denoted as S, representing the total number of yield events. For example, if an avalanche consists of blocks i, j, k failing respectively once, once and twice, then $A = 3$ and $S = 4$. An intuitive way to tune τ_0 is by examining the behaviour of A. Let N_{av} be the number of avalanches measured. Figure 1 illustrates the behaviour of both the maximum ($\max_i A_i$) and average ($\bar{A} = \sum_{i=1}^{N} A_i / N_{\text{av}}$) areas of avalanches for 100 different values of τ_0 thresholds, uniformly distributed between 10^{129} and 2×10^{133} on a logarithmic scale. Avalanches are segmented for a sequence of N_{steps} events. For $\tau_0 \leq 10^{132}$, the maximum exhibits a step-like evolution, with distinct plateaus. In contrast, the average evolves more smoothly and increases over approximately an order of magnitude. In practical terms, even though the largest avalanches roughly retain the same size, their occurrence becomes more frequent as τ_0 increases. For example, when avalanches larger than a fraction $r = 0.005$ of the system size are considered for $\tau_0 = 10^{129}$, 10^{130}, 10^{131}, the corresponding numbers of such avalanches are found to be 108, 366, and 1261, respectively. Beyond $\tau_0 = 10^{132}$, both $\max_i A_i$ and $\bar{A}$ grow rapidly, suggesting that individual avalanches are no longer being effectively segmented. For $\tau_0 \geq 10^{133}$, the avalanches involve almost the entire system, there is no segmentation. The relevance of the choice of τ_0 is also depicted in Fig. 2, where again, a larger threshold induces poor segmentation.

Mainshocks. Mainshocks are identified based on a threshold related to the extent A of avalanches. Specifically, an avalanche characterised A is classified as a mainshock if A exceeds

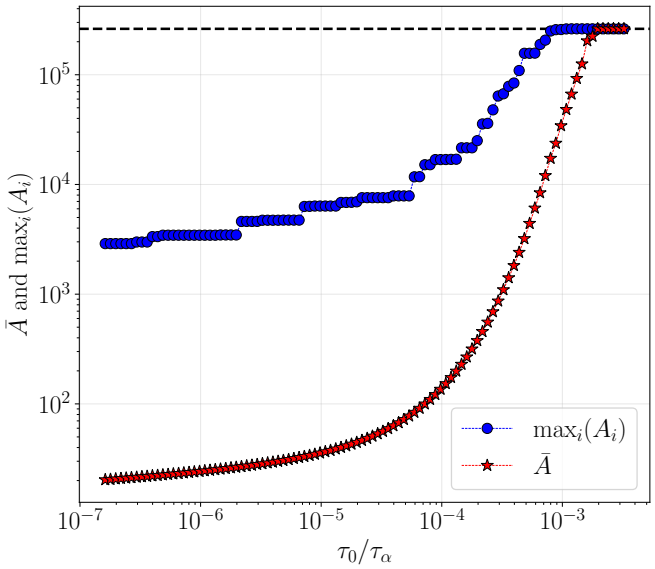

Figure 1: Dependence of both the maximum (blue circles) and the mean (red stars) of avalanche extents A on the time threshold τ_0. For $\tau_0 \geq 10^{132}$, avalanches are less well segmented. After 10^{133} both quantities saturate at the system size L^d indicated by the black dashed line.

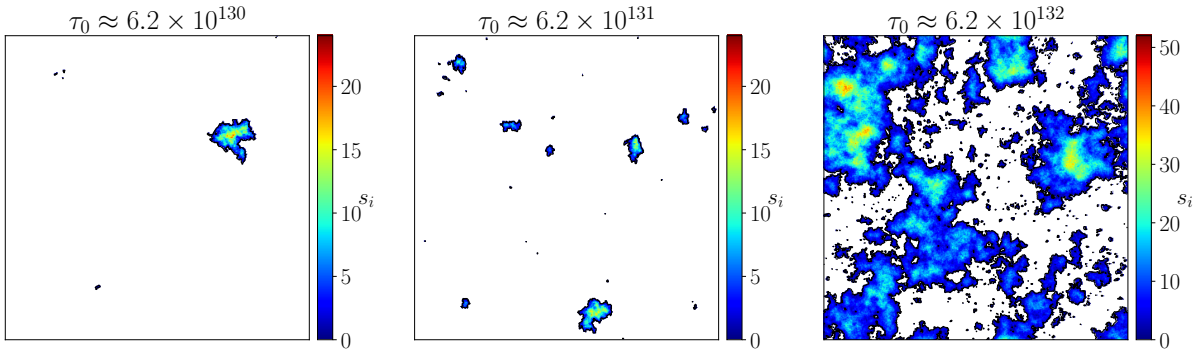

Figure 2: Typical avalanches for three different thresholds τ_0. The colour bar indicates the number of times each individual block fails, denoted by s_i. (a) Below a threshold of $\tau_0 \approx 6.2 \times 10^{130}$, most avalanches form a single connected cluster. (b) As τ_0 increases, a larger number of spatially disconnected events are considered to be part of the same avalanche. (c) For $\tau_0 \approx 6.2 \times 10^{132}$, avalanche segmentation becomes ineffective.

a certain fraction of the total system size, that is, if $A > rL^d$, with $r \in [0, 1]$.

Aftershocks. Following the identification of a mainshock, aftershocks are defined considering the model's assumption of nearest-neighbour interactions. Aftershocks are the events that occur after the mainshock, within the mainshock zone or on adjacent blocks, since force redistribution also occurs on blocks outside the mainshock's boundary. Thus, events are also classified as aftershocks if they are "linked" to the mainshock through preceding aftershocks. The sequence ends as soon as one disconnected event is recorded. Figure 4 illustrates this definition.

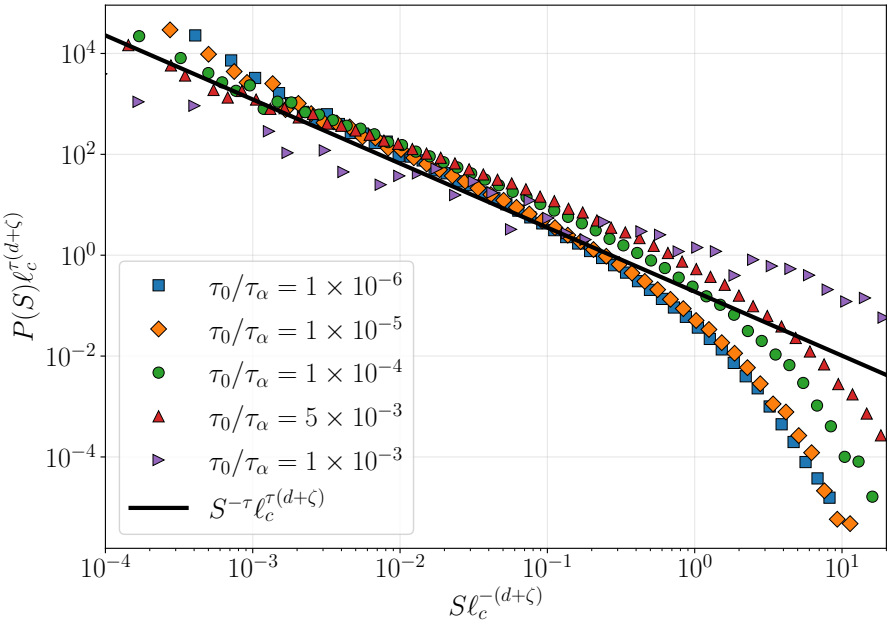

Figure 3: The avalanche size distribution for different values of τ_0 is a power-law cut off by ℓ_c, such that $P(S) \sim S^{-\tau}$ and $S_c \sim \ell_c^{d+\zeta}$. Deviations from the relation can be observed for $\tau_0 \approx 6.2 \times 10^{132}$. The solid line represents a power-law fit with a fixed exponent $-\tau$.

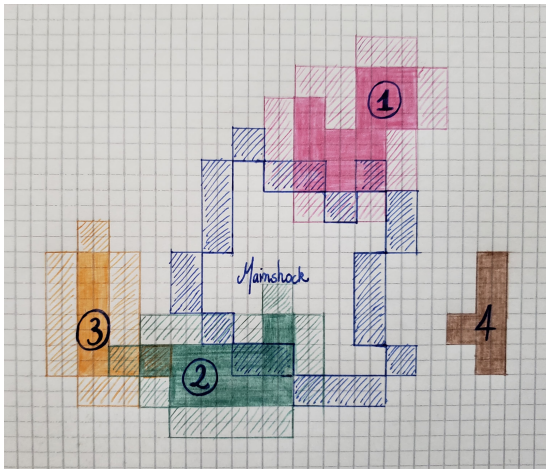

Figure 4: Schematic of aftershock detection. The numbers $i = 1, 2, 3, 4$ represent the chronological occurrence of avalanches following the mainshock. The aftershocks are the events marked with (i). The hatched zones around each event illustrate the areas where force has been redistributed. In this specific example, events 1 and 2 have a direct connection to the mainshock. The third avalanche is linked through the second aftershock. The sequence concludes with the fourth event since it is not connected to preceding aftershocks.

3 Simulations and results

3.1 Examples of mainshocks and their aftershocks.

Two mainshocks obtained for $\tau_0 = \tau_\alpha \times 10^{-4}$ are depicted in Fig. 5. Since our avalanches only take time differences of consecutive events into account, spatially disconnected events happening at the same time are part of the same avalanche. Mainshocks are only defined as large avalanches, thus, they are often made of multiple disconnected clusters. This also explains

why small isolated islands are observed despite most aftershocks being close to mainshock clusters as imposed by our definition. The total number of aftershock clusters is visible through the representation of their centres, which are calculated as a weighted average of the positions of the failing blocks, with weights given by the number of failures s_i for each block.

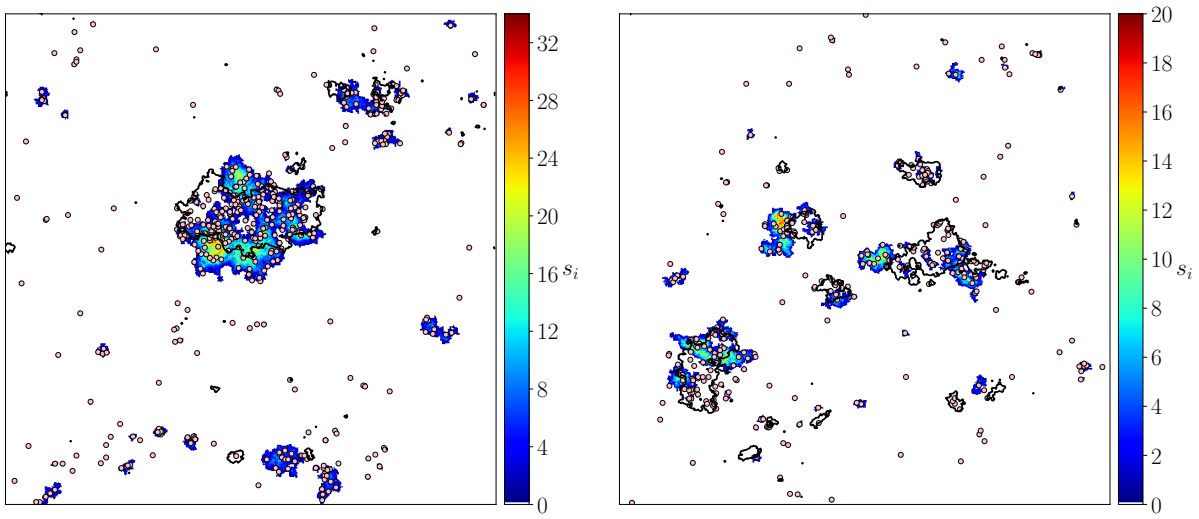

(a) (b)

Figure 5: Mainshocks (outlined in black) and their corresponding aftershocks (depicted with a colour map) obtained with $\tau_0 = \tau_\alpha \times 10^{-4}$. Pink circles represent the centre of each aftershock cluster. The colour bar indicates the number of times s_i that each individual block fails. (a) A mainshock with a dense core; the aftershocks mostly cluster within this area and along its borders. (b) A more dispersed mainshock; the aftershocks are spread out and are located around each component of the mainshock.

3.2 Omori-Utsu law.

The Omori-Utsu law describes the decay in aftershock frequency following a mainshock, typically represented as $n(t) = k(c+t)^{-p}$, where k and c are constants [3]. In this subsection, we investigate whether this decay pattern is mirrored in thermal avalanches of our system. Instead of looking at the frequency, we can integrate it and work with the cumulative distribution $N(t) = \int_0^t n(s)\mathrm{d}s$. For $p = 1$, we find $N(t) = k\ln(1 + t/c)$. For the more general case, $N(t) = k[(c+t)^{1-p} - c^{1-p}]/(1-p)$. Figure 6 illustrates the outcomes for a sequence of N_{steps} events, segmented with a temporal threshold $\tau_0 = \tau_\alpha \times 10^{-4}$ and a mainshock threshold of $r = 0.03$. In this sequence, twenty-five mainshocks were detected. The cumulative number of aftershocks, however, does not align with Omori's law, which predicts a high initial frequency of aftershocks diminishing over time. Instead, the aftershock frequency appears to follow a linear relationship. Intuitively, one might think that this results from a misinterpretation of aftershocks. Since mainshocks can consist of multiple clusters, it might be necessary to also separate the detection of aftershocks for each of them. However, simulations with a lower τ_0, and thus composed of compact mainshocks, also yield an almost linear cumulative distribution.

4 Conclusion

In this report, we have segmented sequences of thermally activated events into avalanches, which enabled us to define mainshocks and aftershocks. Our attempt to apply the Omori-Utsu law

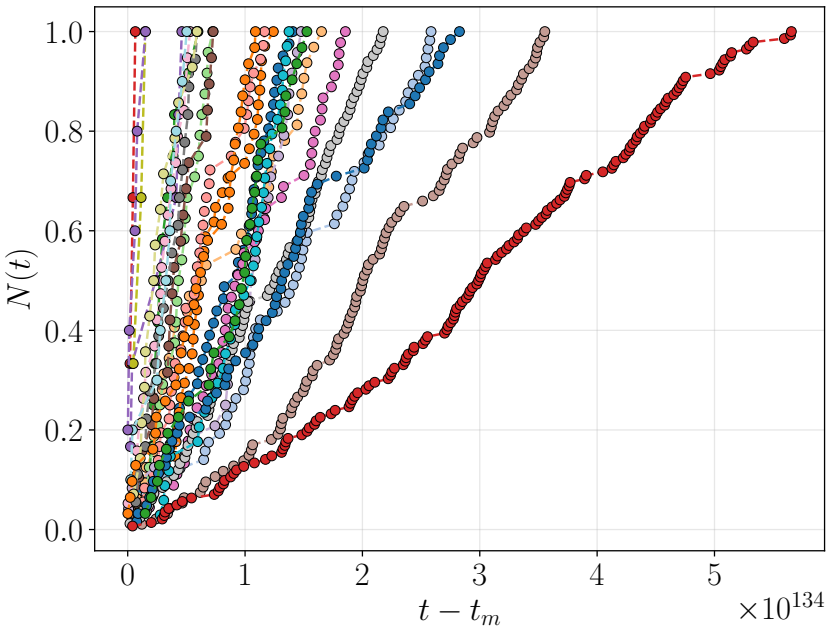

Figure 6: Cumulative distributions of aftershocks following 25 mainshocks. Instead of the anticipated logarithmic or polynomial growth, a linear trend is observed. Each marker represents an aftershock, with t_m denoting the time of the mainshock.

yielded inconclusive results. Despite this, we note that the majority of post-mainshock events are in fact aftershocks, in the sense that they are linked to a mainshock. This suggests that post-mainshock events tend to occur within or near the boundaries of the mainshock zone. Future studies might also consider examining other physical quantities, such as the evolution of the cumulative energy released by aftershocks, or attempt to test the Gutenberg-Richter law.

References

[1] Tom W.J. de Geus, Alberto Rosso, and Matthieu Wyart. "Dynamical heterogeneities of thermal creep in pinned interfaces". 2024. DOI: https://doi.org/10.48550/arXiv.2401.09830.

[2] Tom W.J. de Geus. *GooseEPM*. https://github.com/tdegeus/GooseEPM. 2023.

[3] Tokuji Utsu et al. "The Centenary of the Omori Formula for a Decay Law of Aftershock Activity". In: *Journal of physics of the earth* 43 (1995), pp. 1–33. URL: https://api.semanticscholar.org/CorpusID:13721176.